Electronic Supplementary Material (ESI) for Physical Chemistry Chemical Physics.

Supplementary Information

Low-energy constraints on photoelectron spectra measured from liquid water and aqueous solutions

Sebastian Malerz[1], Florian Trinter[1,2], Uwe Hergenhahn[1,3], Aaron Ghrist[1,4], Hebatallah Ali[1,5], Christophe Nicolas[6], Clara-Magdalena Saak[7], Clemens Richter[1,3], Sebastian Hartweg[6], Laurent Nahon[6], Chin Lee[1,8,10], Claudia Goy[9], Daniel M. Neumark[8,10], Gerard Meijer[1], Iain Wilkinson[11]*, Bernd Winter[1]*, and Stephan Thürmer[12]*

[1] *Molecular Physics Department, Fritz-Haber-Institut der Max-Planck-Gesellschaft, Faradayweg 4-6, 14195 Berlin, Germany*

[2] *Institut für Kernphysik, Goethe-Universität, Max-von-Laue-Strasse 1, 60438 Frankfurt am Main, Germany*

[3] *Leibniz Institute of Surface Engineering (IOM), Department of Functional Surfaces, 04318 Leipzig, Germany*

[4] *Department of Chemistry, University of Southern California, Los Angeles, CA 90089, USA*

[5] *Physics Department, Women Faculty for Art, Science and Education, Ain Shams University, Heliopolis, 11757 Cairo, Egypt*

[6] *Synchrotron SOLEIL, L'Orme des Merisiers, St. Aubin, BP 48, 91192 Gif sur Yvette, France*

[7] *Department of Physics and Astronomy, Uppsala University, Box 516, SE-751 20 Uppsala, Sweden*

[8] *Department of Chemistry, University of California, Berkeley, CA 94720 USA*

[9] *Centre for Molecular Water Science (CMWS), Photon Science, Deutsches Elektronen-Synchrotron (DESY), Notkestraße 85, 22607 Hamburg, Germany*

[10] *Chemical Sciences Division, Lawrence Berkeley National Laboratory, Berkeley, CA 94720, USA*

[11] *Department of Locally-Sensitive & Time-Resolved Spectroscopy, Helmholtz-Zentrum Berlin für Materialien und Energie, Hahn-Meitner-Platz 1, 14109 Berlin, Germany*

[12] *Department of Chemistry, Graduate School of Science, Kyoto University, Kitashirakawa-Oiwakecho, Sakyo-Ku, Kyoto 606-8502, Japan*

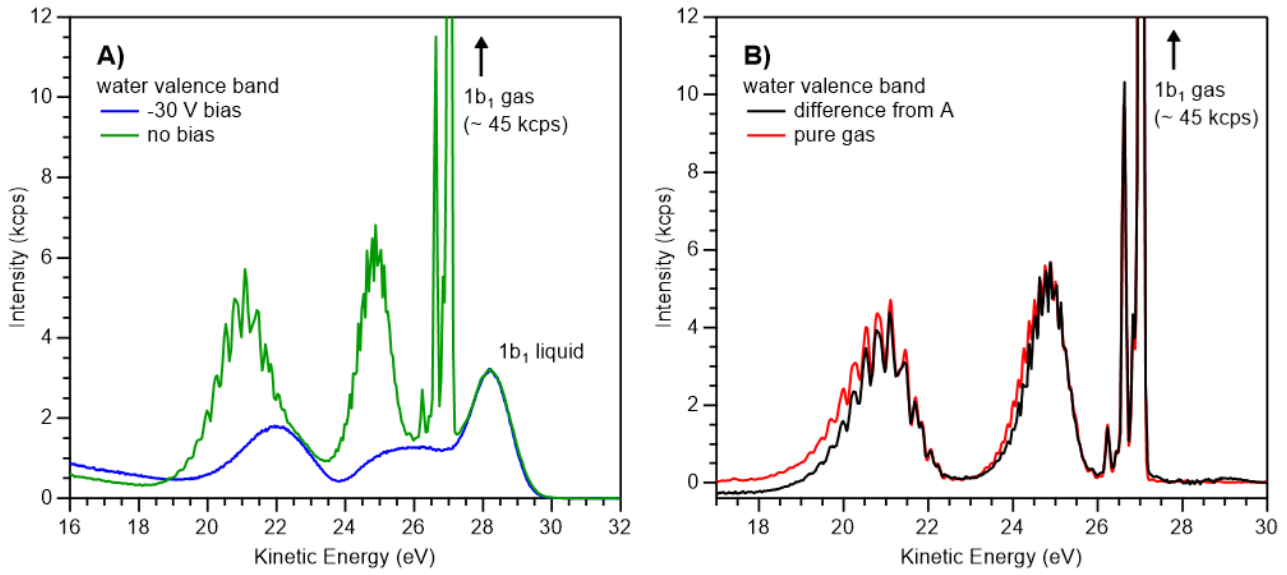

Figure SI-1: A) An exemplary photoelectron (PE) spectrum of the liquid water valence band measured with a He II α emission light source (hν = 40.813 eV). In the case of the blue spectrum, a -30 V bias voltage was applied to the jet, while the green spectrum was measured with a grounded jet. The kinetic energy offset imposed by the bias voltage has been corrected for and the blue spectrum was scaled to yield the same height for the liquid $1b_1$ peak. With the bias applied, the spectrum is almost completely free of gas-phase signal contribution which gets smeared out to lower kinetic energies (before correction for the effect of the bias voltage). The somewhat larger intensity of the blue spectrum for eKE < 20 eV is a consequence of small analyzer transmission changes when measurements are made at the 30 eV higher kinetic energy (KE). **B)** The difference spectrum between the green and blue curves in panel A is shown in black, and a spectrum measured from pure water vapor is shown in red for comparison. The latter spectrum was scaled to the same height and convolved with a Gaussian (width = 0.05 eV) to match the limited experimental resolution of the black difference spectrum.

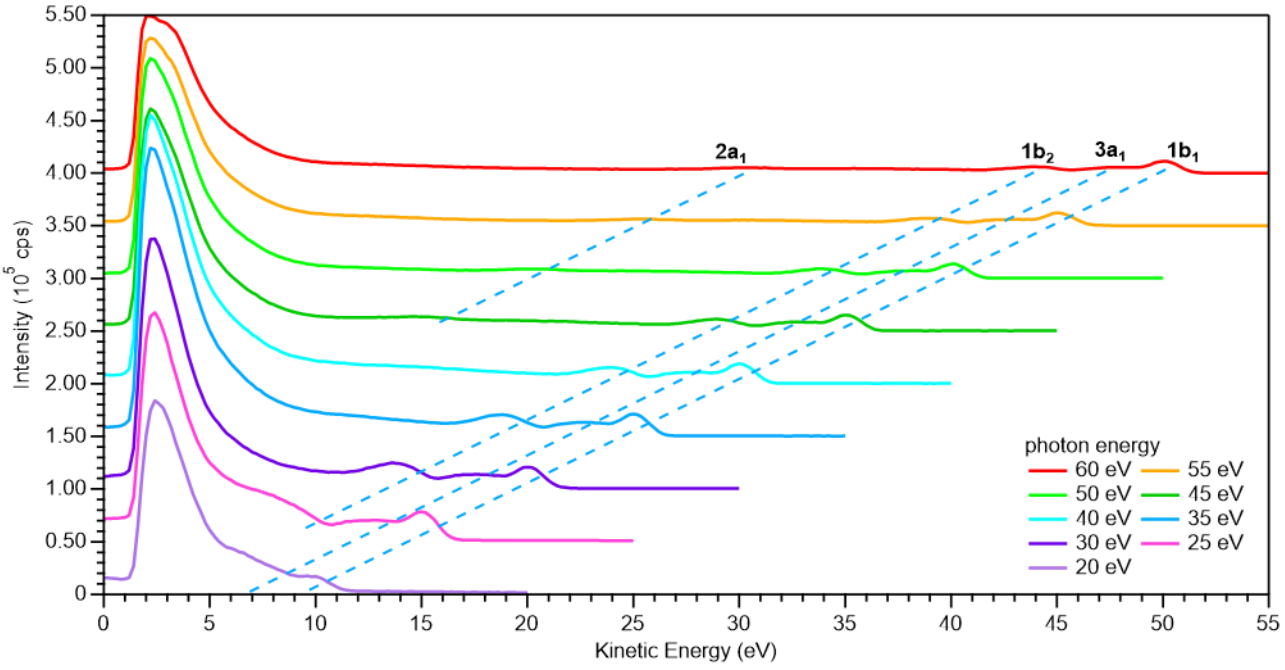

Figure SI-2: The same spectra as shown in Fig. 1 of the main text, but scaled to display the full magnitude of the low-energy tail (LET) curves. Each successive spectrum shown here is offset on the y-axis by 50,000 counts per second (cps).

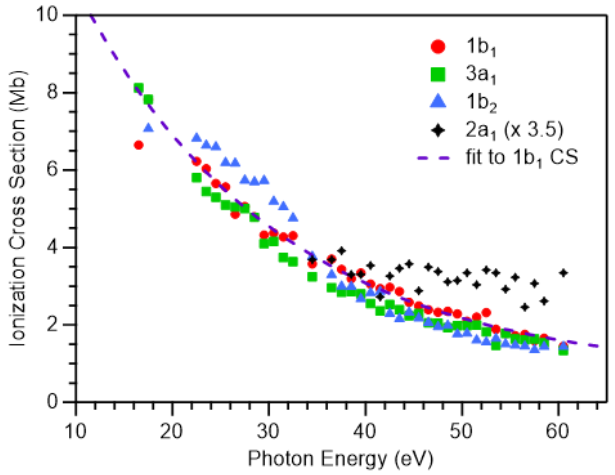

Figure SI-3: Experimental gas-phase photoionization cross sections (CSs) of the $1b_1$ (red circles), $3a_1$ (green squares), $1b_2$ (blue triangles), and $2a_1$ (black diamonds) orbitals from Ref. [1]. The purple dashed line represents an exponential fit of the $1b_1$ CS data; this approximate representation of the photoionization CS of the $1b_1$, $3a_1$, and $1b_2$ orbitals is used for comparison in Fig. 2A in the main text. The data we show here were obtained by electron impact at low momentum transfer, as this is the only available data set covering the threshold region. Photoelectron measurements, available above 30 eV, agree with the former within the scatter of the data.[2]

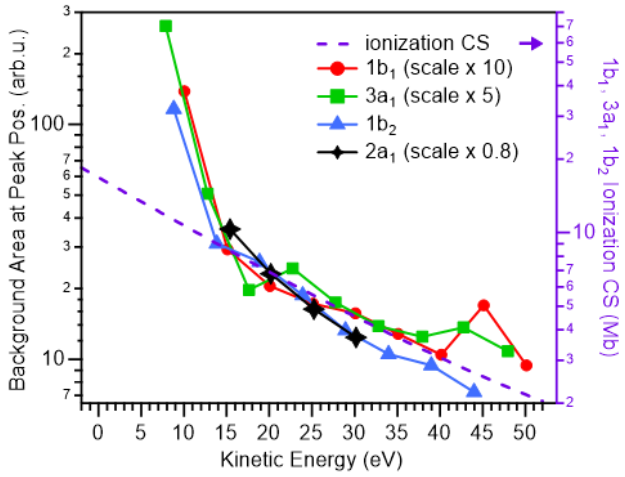

Figure SI-4: Absolute inelastic background signal strength at the respective peak position before normalization to the peak areas (which is shown in Fig. 2B in the main text). Background intensities were extracted at the $1b_1$ (red circles), $3a_1$ (green squares), $1b_2$ (blue triangles), and $2a_1$ (black diamonds) peak positions by integrating over the FWHM of each peak. The signal scaling accounts for the fact that the background below the $2a_1$ ($1b_1$) peak is relatively high (low) due to the peak's relative position in the spectrum. A representation of the ionization cross sections for the $1b_1$, $3a_1$, and $1b_2$ ionization channels from Ref. [1] is overlaid onto the data as a purple dashed line using the scale to the right (see main text and Fig. SI-3). The background smoothly increases proportionally to the CS towards lower eKE until the 10-15 eV region is reached, where it starts to deviate from this trend and rises towards higher intensities.

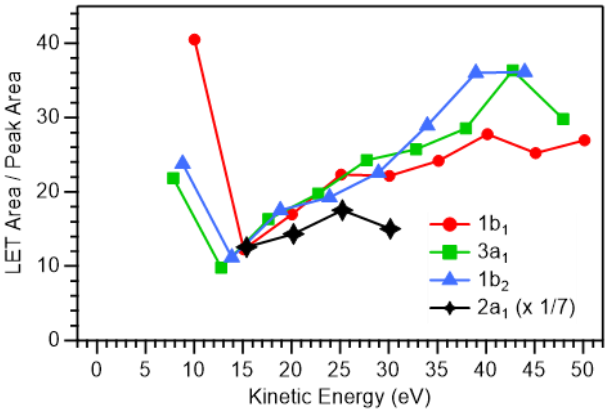

Figure SI-5: Low-electron-kinetic-energy tail, LET, area vs. peak area. The LET was integrated from 1-5 eV after correction for the residual gas-phase contribution and then normalized to (divided by) the $1b_1$ (red circles), $3a_1$ (green squares), $1b_2$ (blue triangles), and $2a_1$ (black diamonds) peak areas.

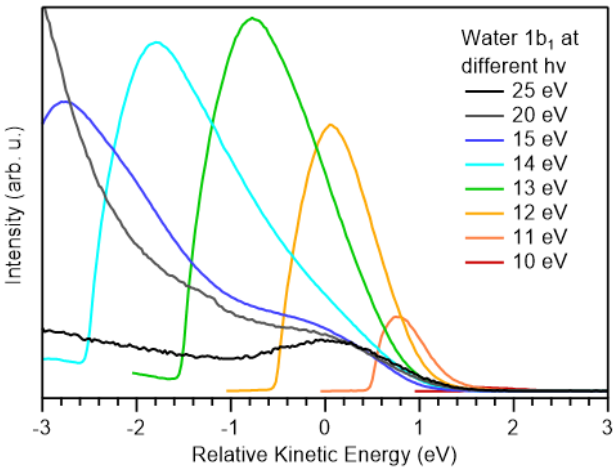

Figure SI-6: Photoemission spectra from liquid water obtained for photon energies of 10-25 eV, which covers energies above and below $VIE_{1b1(l)}$ (= 11.3 eV); the figure is based on the same data as Fig. 3 in the main text. As before, all spectra are shifted so as to compensate for the difference in

photon energy according to hν - $VIE_{1b1(l)}$ ($VIE_{1b1(l)}$ = 11.3 eV). Unlike in Fig. 3, LET intensities are not clipped but rather displayed to yield the approximate relative intensities. For that, spectral intensities have been adjusted for photon flux and for (very approximate) changes in analyzer transmission; the latter is found to be sufficient for our qualitative analysis.

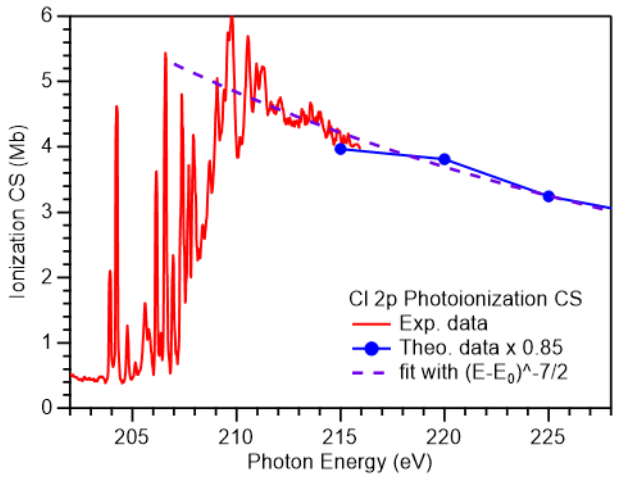

Figure SI-7: 2p photoionization cross sections (CSs) of atomic Cl: Experimental data from Ref. [3] and theoretical data from Ref. [4] scaled by a factor of 0.85. The purple dashed line represents a fit with $(E-E_0)^{-7/2}$ of the experimental CS from 209 eV to 216 eV; this approximate representation of the photoionization CS is used for comparison in Fig. 4D in the main text.

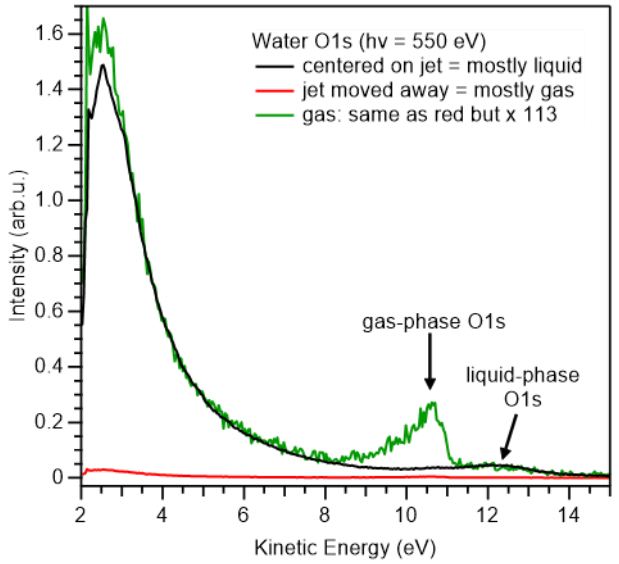

Figure SI-8: Photoemission spectra from liquid and gas-phase water measured at 550 eV photon energy using TOF spectroscopy, exhibiting the respective O 1s photoelectron peaks and LETs. The black curve shows the signal when the overlap between the liquid jet and the X-ray focus is optimized. The red curve was measured when the jet position was shifted sufficiently so that the X-ray spot has almost no overlap with the liquid jet, resulting in almost exclusive ionization of the surrounding gas-phase molecules. The green curve shows the red curve multiplied by a factor 113 which yields matching LET spectra. We find that the small contribution from the liquid phase essentially yields a scaled-down liquid water photoemission spectrum, implying that there is no LET signal generated in the gas phase. Spectra were measured with the magnetic bottle set-up described in conjunction with Fig. 4 of the main text. The asymmetry of the O 1s gas-phase peak results from both vibrational excitations[5] and asymmetric peak broadening due to post-collision interactions.

Estimate of the number of electron - gas-phase water collisions in a liquid-jet PES experiment

In the following we estimate the importance of collisions between electrons emitted from the liquid jet with molecules in the gaseous water surrounding the liquid jet. We assume a sharp gas-liquid interface and a vapor pressure above the liquid corresponding to the equilibrium water vapor pressure of 8 mbar at 4 °C. Furthermore, the gas-phase pressure is taken to drop linearly with distance, *r*, in the radial direction from the water-jet surface. The distance between the jet and the skimmer at the entrance of the electron spectrometer is taken as r_1 = 0.5 mm, and collisions after electrons have passed the differentially pumped skimmer aperture are considered unimportant. We can then estimate an effective vapor column μ (with the dimension of (particle number density) * length = inverse area, i.e., cm^{-2}) which characterizes the integrated gas density the electrons have to pass before being detected, according to Ref. [6]:

$$\mu(r_0, r_1) = \int_{r_0}^{r_1} dr\, n_0 \frac{r_0}{r} = n_0 r_0 \ln\left(\frac{r_1}{r_0}\right) \qquad (1).$$

Here, r_0 is the jet radius and n_0 is the particle number density at the liquid-vapor interface. Inserting r_0 = 12.5 µm and r_1 = 500 µm, we arrive at $\mu \sim 1 \times 10^{15}$ cm^{-2}. Using the Lambert-Beer law in the

following form to determine the intensity reduction of a beam passing some medium:

$$I = I_0 \exp(-nl\,\sigma) \qquad (2),$$

with I_0 and I describing the original and the reduced intensity, n and l the density and path length through the medium, and σ the cross section for some scattering process, we can insert our estimated value ($\mu \sim 10^{15}$ cm^{-2}) of the effective vapor column in place of nl. Taking for example the cross section of some inelastic process as 10^{-16} cm^2 (100 Mb), we then calculate a 90% ($\exp(-0.1) \cong 0.9$) transmission of the electron beam. Thus, the sudden drop in liquid-phase peak intensity in the 10-13 eV region cannot be explained by scattering in the gas phase, especially since the electronic scattering channels responsible for reducing the peak intensity decrease in this electron kinetic energy region.

It is interesting to note that the exponential term in Eq. (2), $\exp(-nl\,\sigma) = \exp(-0.1)$, can be interpreted as the $P(k = 0)$ value of the Poissonian probability distribution for the number of collisions, k, encountered by an electron on its path through the gas phase, written as:

$$P_\lambda(k) = \frac{\lambda^k}{k!}\exp(-\lambda) \qquad (3).$$

Here, λ is the probability parameter. The argument of the exponential function thus corresponds to the average number of collisions encountered due to the process with cross section σ. We have 0.1 collisions for a σ of 10^{-16} cm^2. In view of the value of μ estimated above, it is seen that only processes with cross sections exceeding 1000 Mb can lead to an appreciable number of collisions, under the assumptions given above. Referring to the rich literature on electron scattering on gas-phase H_2O, we find that only elastic or quasi-elastic scattering involving molecular rotation may reach cross sections in that range. The latter scattering processes may influence the angular distribution function, but will not lead to significant changes in the kinetic energy of the electrons. Thus, for primary electrons of several tens of eV, the contribution to the inelastic background and LET must be small. Indeed, we do not find any contribution of the gas-phase water molecules to the measured LET, as demonstrated in Fig. SI-8.

References

1. K. H. Tan, C. E. Brion, Ph. E. Van der Leeuw and M. J. van der Wiel, *Chem. Phys.*, 1978, **29**, 299-309.
2. M. S. Banna, B. H. McQuaide, R. Malutzki and V. Schmidt, *J. Chem. Phys.*, 1986, **84**, 4739-4747.
3. W. C. Stolte, Z. Felfli, R. Guillemin, G. Öhrwall, S. W. Yu, J. A. Young, D. W. Lindle, T. W. Gorczyca, N. C. Deb, S. T. Manson, A. Hibbert and A. Z. Msezane, *Phys. Rev. A*, 2013, **88**.
4. J.-J. Yeh, *Atomic Calculations of Photoionization Cross Sections and Asymmetry Parameters*, Gordon & Breach, Langhorne, PA, USA, 1993.
5. R. Sankari, M. Ehara, H. Nakatsuji, Y. Senba, K. Hosokawa, H. Yoshida, A. De Fanis, Y. Tamenori, S. Aksela and K. Ueda, *Chem. Phys. Lett.*, 2003, **380**, 647-653.
6. M. Faubel, S. Schlemmer and J. P. Toennies, *Z. Phys. D: At., Mol. Clusters*, 1988, **10**, 269-277.